Plasma exposure of a pre-damaged ITER-like plasma facing unit in the WEST tokamak: in-situ and post-mortem measurements

Yann Corre, Torsten Loewenhoff, Marianne Richou, Sebastijan Brezinsek, Jan Coenen, Renaud Dejarnac, Mathilde Diez, Nicolas Fedorczak, Mehdi Firdaouss, Jonathan Gaspar, et al.

Nuclear Materials and Energy 34 (2023) 101366

Contents lists available at ScienceDirect

Nuclear Materials and Energy

journal homepage: www.elsevier.com/locate/nme

Plasma exposure of a pre-damaged ITER-like plasma facing unit in the WEST tokamak: in-situ and post-mortem measurements

Yann Corre [a,*], Torsten Loewenhoff [b], Marianne Richou [a], Sebastijan Brezinsek [b], Jan Coenen [b], Renaud Dejarnac [c], Mathilde Diez [a], Nicolas Fedorczak [a], Mehdi Firdaouss [a], Jonathan Gaspar [d], Alex Grosjean [a], James-Paul Gunn [a], Thierry Loarer [a], Céline Martin [e], Gerald Pintsuk [b], Pierre Reilhac [a], Quentin Tichit [a], Emmanuelle Tsitrone [a], Marius Wirtz [b], the WEST team [f]

[a] CEA, Institute for Research on Fusion by Magnetic confinement, 13108 St-Paul-Lez-Durance, France
[b] Forschungszentrum Jülich GmbH, Institut für Energie und Klimaforschung 52425 Jülich, Germany
[c] Institute of Plasma Physics, Czech Academy of Sciences, 182 00 Prague, Czech Republic
[d] Aix-Marseille Univ, CNRS, IUSTI, Marseille, France,
[e] Aix-Marseille Université, CNRS, PIIM UMR 7345, F-13397 Marseille, France
[f] See http://west.cea.fr/WESTteam

ARTICLE INFO

Keywords:
Damaged PFC
ITER like tungsten PFC
Heat load
IR thermography
Heat transfer modelling

ABSTRACT

The consequences of tungsten (W) cracking on divertor lifetime and plasma operation are high priority issues for ITER. One actively cooled ITER-like plasma facing unit (PFU) has been pre-damaged in a High Heat Flux (HHF) facility before its installation in WEST in order to assess the damage evolution after tokamak plasma exposure. The resulting pre-damage exhibits micrometer-size crack network and high roughness on the tungsten monoblock (MB) top surface. A total of 10 MBs, equally distributed on the low and high field sides of the lower divertor, have been pre-damaged among the 35 radially aligned MBs characteristic of the WEST PFU. Subsequent plasma exposure was carried out, from the first breakdown achieved in WEST (in 2017) until the removal of the damaged PFU three years later (2020). On top of the whole WEST plasma exposure (covering C1-C4 experimental campaigns), a dedicated experiment has also been performed in the frame of the EU work program to maximize the power and energy loads on one of the damaged MBs featuring a "crack network" pattern. The MB top surface, including both "crack network" damage and "healthy" (undamaged) areas, was monitored with a high spatial resolution IR camera to detect any potential evolution of the damage pulse after pulse. This paper describes the full plasma exposure achieved in the WEST tokamak (including large number of steady-state and transient heat loading cycles), the dedicated "damaged PFU exposure" experiment together with the experimental results (heat loading on the damaged MBs). Post-mortem measurement reveals significant broadening of the cracks and new cracks in the electron beam loaded area only.

Introduction

Assessing how material damage can form and propagate in an ITER divertor Plasma facing Unit (PFU) under tokamak plasma exposure is an important topic to address for future ITER divertor operation. The assumption in the ITER Research Plan is that the ITER divertor lifetime should be longer than 10 years [1,2], which corresponds to a very large exposure time for plasma components covering the first plasma campaign (1 month), pre-fusion (39 months in hydrogen/helium plasmas) and fusion (48 months of DT plasmas) power operation. Investigating the evolution and potential degradation of ITER grade Plasma Facing Components (PFCs) in a fusion device environment is one of the key mission of the WEST tokamak [3], complementing studies performed in HHF facilities and linear devices [4]. In the first phase of WEST operation, few ITER-like divertor PFUs have been installed and tested on the lower divertor (referred here as the test divertor sector). One of these PFUs has been pre-damaged using the JUDITH 2 HHF facility [5], using thermal shocks cycling to mimic the impact of 10^5 transients of up to 0.55 GW.m^{-2} and a duration of 0.5 ms in ITER, before its installation in WEST in 2017. Three kind of damage have been

* Corresponding author.
E-mail address: yann.corre@cea.fr (Y. Corre).

https://doi.org/10.1016/j.nme.2023.101366
Received 29 July 2022; Received in revised form 21 December 2022; Accepted 11 January 2023
Available online 21 January 2023

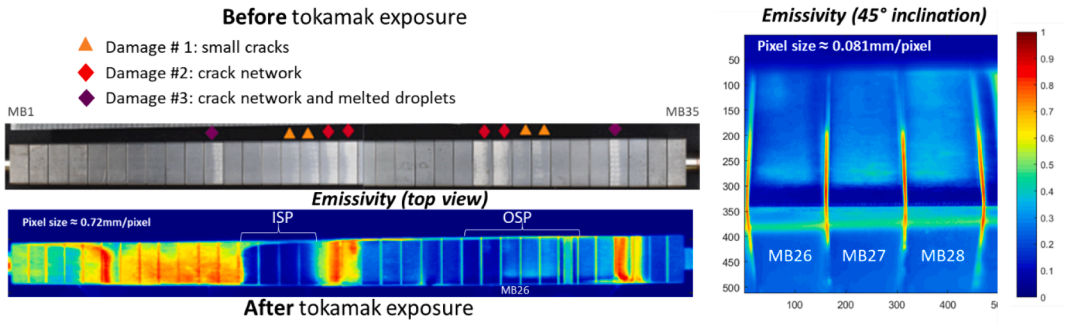

Fig. 1. Pre-damaged PFU before the installation in WEST, including small cracks (MB15, 16, 27, 28), crack network (MB17, 18, 25, 26) and crack network and molten droplets (MB11 and 32) damage type. Zoom on MB26 is presented on the right picture with 45° inclination to see the exposed leading edge.

generated varying the heat flux impact factor from 3 to 12 $MW/m^2 \bullet s^{0.5}$. The damaged W grade exhibits small cracks (damage #1), crack network (damage #2) and crack network plus molten droplets (damage #3) distributed over 10 out of 35 MBs constituting one full PFU in WEST. The damage procedure and the PFU characterization performed before exposure in WEST are presented in [6]. The location of the damage on the PFU are shown in Fig. 1 as function of the MB number from 1 (on the high field side) to 35 (on the low field side). Subsequent plasma exposure was carried out in WEST first, with modest heat load (<1 $MW.m^{-2}$) to avoid compromising the C3 experimental campaign (pre-damaged PFU located in minimum heat flux area on the outer strike point). Since no significant surface aspect modification was found [6], it was decided to move the pre-damaged component to the highest heat load area for the following experimental campaign (C4). The goals of this study were to monitor the damage propagation under tokamak operation, evaluate the consequence for plasma operation with damaged PFCs, get feedback on the measurement capabilities and compare with results obtained with HHF testing facilities. Emissivity measurement performed on the pre-damaged PFU after full tokamak exposure (C1-C4) is shown in Fig. 1 to illustrate the plasma footprint, including erosion area (low emissivity) on the inner (ISP) and outer (OSP) strike point positions and material deposition (high emissivity) in the private, far SOL and magnetically shadowed areas [7]. On the top surface of the damage area, the mean value obtained at 50 °C is 0.27 ± 0.02. After plasma exposure, the emissivity on the pre-damage (loaded by the e-beam) and "healthy" areas (unloaded by the e-beam) are very close, higher than the one measured on pristine tungsten (below 0.1) [8].

The paper is organized as follow. The experimental set-up and WEST experiments are presented in section 2. Section 3 shows the exposure of damaged PFC experiment, the heat load calculation and the very high spatial IR data. The last section shows the preliminary post-mortem analysis (confocal microscopy) after 3 years of tokamak exposure (about 6 h of cumulated plasma duration).

WEST experiments overview (C1-C4 experimental campaigns)

In WEST, each PFU is made of 35 W monoblocks (see Fig. 1) of individual size 12 mm × 26 mm (depth × height), toroidal width varying from 28 to 32 mm on the high and low field sides, respectively, assembled with a gap of 0.5 mm on a CuCrZr heat sink tube [9]. During its first phase of operation, WEST was equipped with upper and lower divertor coils, W-coated upper divertor, baffle, inner bumper and with a flexible lower divertor made of twelve 30° sectors. One of them was equipped with actively cooled ITER-like PFUs (the test divertor sector) and the others were equipped with ineritially cooled W-coated graphite PFUs to complete the divertor ring. The additional heating and current drive power is provided by high frequency heating systems, namely ion cyclotron resonance heating (ICRH) and lower hybrid current drive (LHCD), capable to deliver a nominal power up to 9 MW and 7 MW respectively. The WEST magnetic configurations allow for elongated plasmas in lower or upper single null, or double null configurations. For

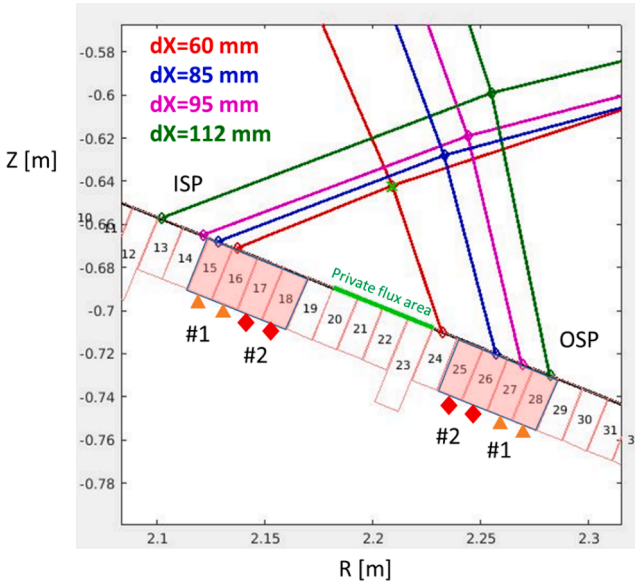

Fig. 2. Lower single null magnetic configurations (B = 3.7 T) used in WEST: from close to far X-point (#54721 in red, #56697 in blue, #54934 in magenta, #56541 in green).

a standard elongated lower single null case, the X-point height ranges from 60 mm for standard operation up to 112 mm, see Fig. 2 (green curve), for dedicated high power operation [10]. According to the X-point height, the separatrix can reach different MBs on the inner and outer strike points as illustrated in Fig. 2. In the ISP area, MB 11 featuring crack network and molten droplets (damage #3) can be reached with very far X-point configuration (X point height > 110 mm) only, MB 15 and 16 featuring small cracks (damage #1) can be reached with standard X-point configuration while MB 17 and 18 featuring crack network (damage #2) can be reached with the close X-point configuration (X point height < 50 mm). In the OSP area, MB 27 and 28 featuring small cracks (damage #1) can be reached with far X-point configuration (X point height > 90 mm) while MB 25 and 26 featuring crack network can be reach with medium X-point height (between 70 and 90 mm).

In its first operation phase with a mix of actively cooled and inertial components, WEST has performed four experimental campaigns, from C1 (2017) to C4 (2019) [11]. The first one was dedicated to the commissioning of the machine and plasma breakdown strategy (C1) [12]. The second one (C2) was dedicated to the increase of the plasma current, development of the X-point magnetic configuration and increase of the auxiliary heating systems (ICRH and LHCD). The last two experimental campaigns were dedicated to physics studies and performance improvement (C3 and C4). The main achievements performed in WEST Phase I are summarized in Table 1. WEST had cumulated about 6

Table 1
Summary of the main achievements performed in WEST phase I: number of plasma, plasma current (Ip), maximum pulse duration, cumulated plasma duration, number of disruptions, total energy injected with LHCD/ICRH systems, position of the pre-damaged PFU on the test divertor sector (see Fig. 3).

	Nb Plasma	Ip max (kA)	Duration max (s)	Cumul (s)	Disruptions	LH total energy (MJ)	IC total energy (MJ)	Pre-damaged PFU position
C2 Nov17-Feb18	716	805	10.5	1553	282	95.5	0	PFU20
C3 July-Dec18	1076	818	37.5	7302	730	4947	105	PFU20
C4 – D2 July-Nov19	1157	1004	55	9968	755	7823	1139	PFU7
C4 - He Oct-Nov19	345	709	29	2991	275	4300	3	PFU7

h of plasma exposure and 17 GJ of injected energy. The standard scenario was a lower single null configuration, L-mode operation with divertor peak heat flux up to ~ 5 MW/m^{-2} as measured on the W-coated graphite PFUs [13]. About 2600 plasma experiments have been successfully achieved. On top of that, a large number of transients (mainly disruptions) was also reported (~2000 transients), each producing thermo-mechanical stresses in the PFCs. Inspection of the components after the campaign revealed a wide variety of damage at both leading and trailing monoblock edges [14] where magnetic field lines strike the MB surfaces with nearly perpendicular incidence angle. Cracking, deformation, and melting occurred.

The monoblocks with damage #1 and #2, located in usual strike point areas, were exposed to most of the discharges of the C3 campaign while a few discharges, requiring a dedicated magnetic configuration, were performed to load the block with the most intense damage #3 on the high field side. Divertor steady state heat fluxes reached during the C3 campaign (<1 MW/m^{-2} on the top surface of the pre-damaged blocks, on the ISP side because of the toroidal field ripple modulation as shown in Fig. 3-b) and corresponding temperatures were moderate [6]. As expected with regard to the heat loading conditions, no major surface aspect modification due to the WEST plasma exposure was found. It was therefore decided to move the pre-damaged component to the highest heat load area for the following experimental campaign (C4), taking advantage of the in/out asymmetry in divertor load. The pre-damaged PFU was therefore moved from PFU20 to PFU7 on the test divertor sector (see Fig. 3), corresponding to a maximum heat flux on the OSP.

High power test of ITER PFC: Exposure of damaged PFC (C4)

Test divertor configuration:

For the C4 experimental campaign, the test divertor sector was equipped with 14 actively cooled ITER-like (flat top, unshaped geometry) and 24 inertially cooled W coated PFUs (0.5 mm toroidal bevel, shaped geometry) as shown on Fig. 3-a. The damaged MBs are shown with the same symbols as used in Fig. 1 to distinguish the damage type (#1, #2, #3). Fig. 3-b displays the heat load pattern modelled with the field line tracing code PFCflux [15] on the test divertor sector during typical plasma exposure experiment (Far X-Point configuration with dX = 85 mm, 500 kA of plasma current, 4 MW auxiliary power injected in deuterium plasma, #55058 performed in C4). The simulation was performed with heat flux decay length λ_q = 10 mm and outer/inner heat flux asymmetry of 4 in the divertor (1/4 on the inner, ¾ on the outer) as measured with embedded thermal measurement [13]. The plot shows the toroidal modulation of the heat flux which is observed with a 20° periodicity due to the toroidal ripple effect of the magnetic field. With the C4 divertor configuration, the MBs 24 to 28 are in the high heat flux area in the OSP, while MBs 15 to18 are in the minimum heat flux area on the ISP.

C4 experimental campaign

The C4 experimental campaign is characterized by a large number of plasma (about 1500) with a significant increase of plasma power and

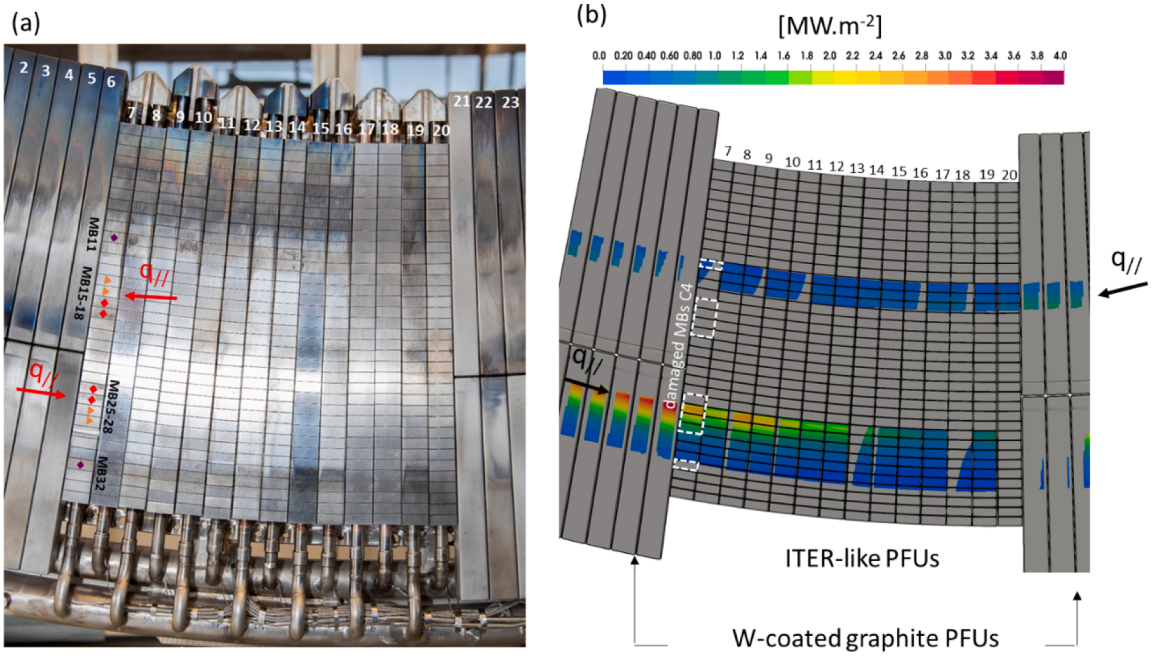

Fig. 3. (a) Test divertor sector installed during C4 experimental campaign, PFU numbers are given in white. (b) PFCflux simulation of the heat load with FXP magnetic equilibrium #55058 (dX = 85 mm, λ_q = 10 mm on the target, P^{SOL} = 1 MW). Damaged PFU is located in PFU7.

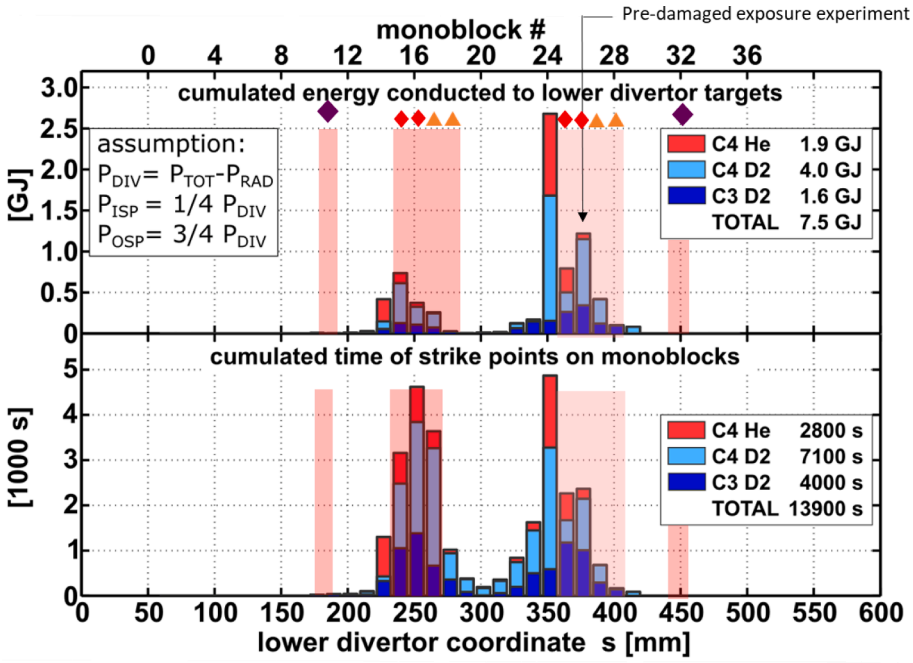

Fig. 4. Accumulated energy estimated at the OSP location and time duration in the C3 and C4 experimental campaigns: helium (red), deuterium (blue) for each MB.

energy compared to C3 (5 and 12 GJ cumulated injected energy in C3 and C4, respectively), plasma duration (800 and 1300 s cumulated plasma duration in C3 and C4 respectively) combined with a high disruption rate (67 %), see Table 1. The first part of the campaign has been performed with deuterium whilst the last two weeks have been performed with helium gas fueling. In this condition, different plasma wall interaction processes (in particular erosion and deposition pattern) have been identified and reported in [16]. Different X-point heights have been used, resulting in different inner and outer strike point locations and consequently different MB exposure (from MB 14–17 and MB23-28 for the ISP and OSP respectively, as displayed in Fig. 4). During C4, higher heat load on the divertor components and longer pulse duration were achieved compared to C3. Fig. 4 shows the cumulated energy received by the lower divertor, computed as function of the strike point position, during the deuterium (blue) and helium (red) parts of the C3 and C4 campaigns. The cumulated energy received by the lower divertor is obtained using the WEST data base as depicted in [13].On the OSP, MB24 (with no pre-damage) is the most loaded under deuterium plasma. This corresponds to the location of the OSP with the most standard magnetic equilibrium. The second most loaded is the MB26 featuring crack network pre-damaging. The total cumulated plasma duration with the OSP located on MB26 is ~ 2200 s. MB25 and MB27 are moderately loaded and MB28 weakly loaded with deuterium plasma. MB24 and MB25 are the most loaded under helium plasma. On the ISP, the MB15 and MB14 are the most loaded in deuterium and helium plasma. The study presented in this paper focuses on the OSP, which is more loaded because of the inner and outer heat flux asymmetry (¾ on the outer).

Repetitive exposure of the ITER pre-damage PFU

A robust steady state plasma scenario has been developed to maximize the power and energy load on one of the pre-damaged MBs featuring the crack network pattern. A series of dedicated high power steady state plasma discharges was performed in the frame of the EU work program, using a very high spatial resolution IR instrument (0.1 mm / pixel) to monitor the surface temperature on the pre-damaged MB. The X-point height was set to 85 mm from the target to put the OSP on MB26 with damage #2 (crack network). The reference pulse duration for these studies is typically 27 s, in which LHCD systems delivers 4 MW steady-state power during 20 s. Plasma parameters are: plasma current Ip = 500 kA, toroidal magnetic field B = 3.6 T, line-averaged density, $<n_e>$, in the range of 3.8 to 4 × 10^{19} m^{-2}. The radiated power fraction (f^{rad}) is in the range of 55 to 60 %. Injected and radiated power are shown in Fig. 5 for a typical shot repeated during the experimental sessions. Each exposure shot corresponds to about 90 MJ of cumulated energy delivered to the plasma (ohmic and RF powers). After the experimental session, about 600 s and 1.9 GJ of cumulated plasma exposure time and energy delivered to the plasma have been reached using the same magnetic equilibrium and plasma settings. This represents a significant proportion of the total cumulated plasma exposure on MB26 (~2200 s) and also energy delivered to the plasma (17 GJ).

About 30 plasma discharges have been repeated and no consequence on the plasma operation were observed. A slow and tiny increase of plasma radiation pulse to pulse has been observed, leading to a decrease of the divertor power during the sessions. W sources have been monitored on the pre-damaged PFU with visible spectroscopic system [17].

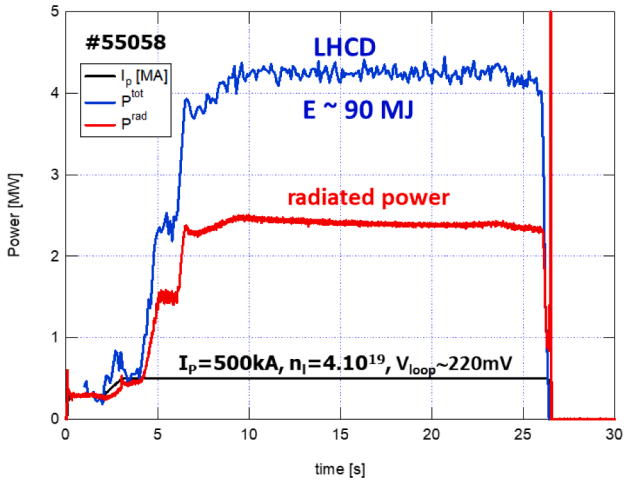

Fig. 5. Pulse scenario achieved for the high power exposure of ITER-like PFC: total injected power (ohmic + RF heating in blue), radiated power (in red) and plasma current in black.

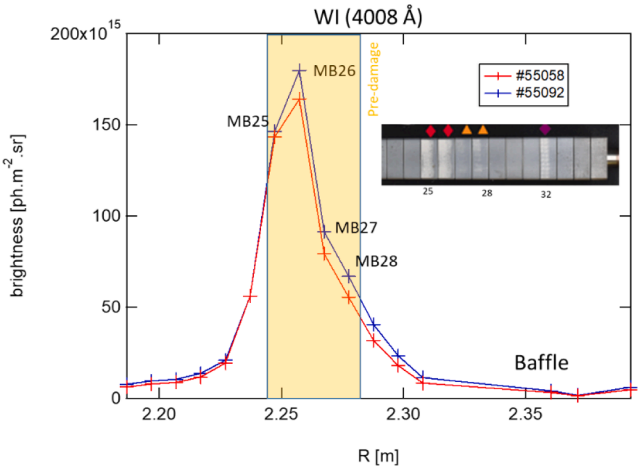

Fig. 6. WI emission measured before (red, #5058) and (blue, #55092) after the dedicated and repetitive plasma exposure.

The optical telescopes have 10 mm spatial resolution which is close to one MB width (12 mm). Experimental data are displayed in Fig. 6 for two similar pulses, one of the first (red) and one of the last (blue) pulse of the dedicated exposure session. The WI emission profiles do no exhibit any significant evolution after dedicated plasma exposure. A slight increase of the WI emission is observed, which is consistent with the results mentioned above with the total radiated power.

The heat loads are computed using different sensing technologies (FBGs, TCs, LPs, IR thermography), embedded in, or looking at the W-coated graphite PFUs as depicted in [13,18,19]. The heat load profile is modelled by the convolution of a Gaussian in the private flux side with an exponential function in the SOL side as depicted in [13] (S being the spreading factor and λ_q the heat flux decay length). Fig. 7 displays the peak heat flux (a) and target heat flux decay length (b) as function of the power reaching the divertor. The peak heat fluxes measured on the top surface of the PFUs are found to be in the range of 1.7 – 3.2 MW.m^{-2} in the "high power" regime (when $P^{div} = 1.8 \pm 0.2$ MW, orange area, Fig. 7-a). The average values for the target heat flux decay lengths are $\lambda_q = 12 \pm 3$ mm and $\lambda_q = 25 \pm 5$ mm with standard IR thermography and embedded sensors respectively. For the two derived parameters, peak heat flux (a) and heat flux decay length (b), the data scattering is quite large and could be explained by different reasons: the sensing technologies and the performances of the diagnostics are different (in particular the spatial resolution), the toroidal location of the sensors are also different in the lower divertor (even if the position regarding the toroidal magnetic ripple is the same) and the plasma properties can differ from pulse to pulse because of MHD activity, RF power coupling, impurity content and transport properties (turbulence) that could result in different electron and ion plasma temperature at the target for similar P^{div}.

The pre-damaged PFU exhibits a 1 mm poloidal chamfer and a flat top surface geometry (there is no shaping on this PFU, the opposite as it is foreseen in the ITER divertor [20]). At the OSP, the incident angle of magnetic field lines with the top surface and 1 mm chamfer are $\alpha_{top} = 2.4°$ and $\alpha_{ch} = 47.4°$ respectively (#55058). The heat flux on the top surface, the 1 mm chamfer and the poloidal leading edge of the block are computed with the optical approximation (OA):

$$q_n = q_{||} sin\alpha \quad (1)$$

Where $q_{//}$ is the parallel heat flux and α is the incident angle of the magnetic field with the different MB surfaces. Due to the radial misalignment of ~ 0.2 mm of the PFU7 with regard to PFU6 (previous PFU regarding the plasma flow on the OSP), the chamfer of the leading edge is partially exposed to the plasma heat flux. Using geometrical consideration and equation (1), the heat load on top surface and exposed chamfer of MB 26 are ~ 2.4 MW.m^{-2} and ~ 55 MW.m^{-2}, respectively. In complement to the IR data measurement, the temperature of the 28 mm width monoblock is also calculated with Finite Element Modelling (ANSYS code) using numerical heat fluxes (eq. (1)), both on chamfers sides and on the top surface. The calculation is made on ITER-like MB prototypes with 28 mm width and 6 mm tungsten thickness between the top surface and the CuOFHC joint covering the CuCrZr heat sink actively cooled with pressurized water (water temperature = 70 °C, speed = 10 m.s^{-1} and pressure = 3 MPa). An iterative loop is used to find the best S and λ_q that matches both the poloidal and toroidal experimental temperature profiles (see section 3.4).

Surface temperature measurement

The surface temperature map measured with the Very High Resolution (VHR) IR system [21] during the dedicated exposure experiment is displayed in Fig. 8 assuming surface emissivity of 0.3 as extrapolated from the post-mortem analysis on the pre-damaged PFU. The emissivity measurement was performed in laboratory at 50 °C [22]. The experimental emissivity values are extrapolated to the temperature obtained during the plasma experiment assuming an increase of emissivity of 10^{-4} per degree [8]. On the poloidal leading edge chamfer (located on the left side on the IR image), the temperature is about 800 °C. On the middle of the MB, right above the cooling pipe, the temperature is found to be quite homogenous, typically between 380 °C and 400 °C. The cracks generated by the electron beam in the HHF test facility are of the order

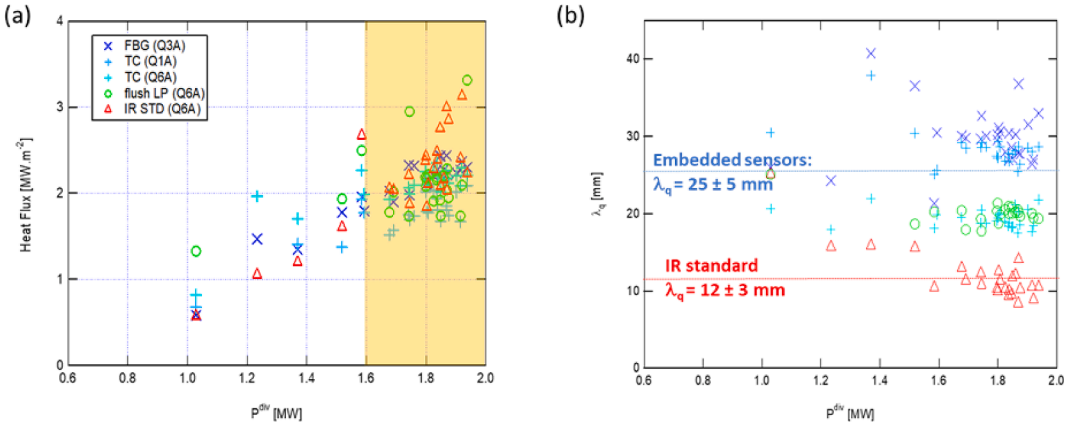

Fig. 7. Peak heat flux (a) and target heat flux decay length (b) measured on the top surface of the PFU using different sensing technologies: embedded fiber Bragg grating (FBGs), thermocouples (TCs), Langmuir probe (LP) and standard IR thermography as function of the power reaching the divertor. The high power operation domain is shown in orange in figure (a).

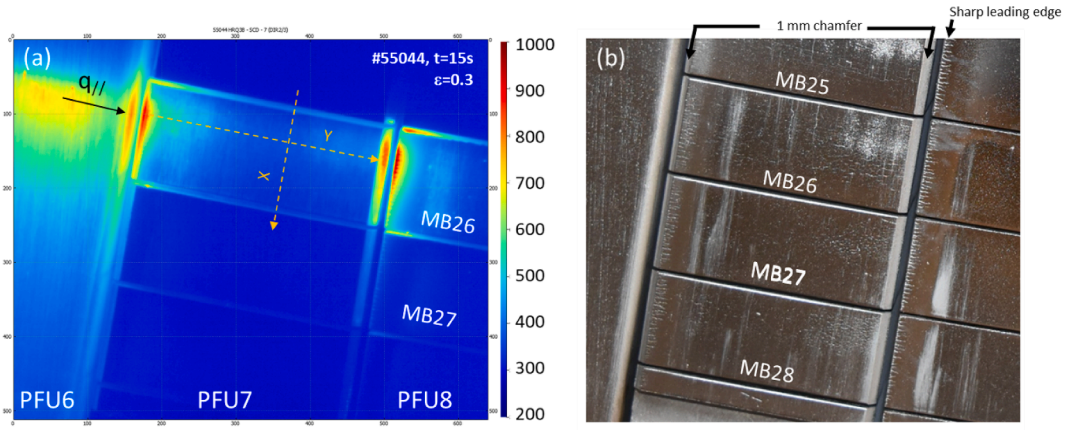

Fig. 8. (a) Surface temperature measured by the VHR IR system at t = 15 s, when the thermal equilibrium of the PFU is reached. (b) Picture of the –pre-damaged PFU taken after the C4 experimental campaign (2019).

of few tens of micrometers size. Because of the finite pixel size (0.095 mm/pixel in the object plane) and the optical blurring and deformation [23], such cracks are too small and not visible with the VHR IR system. The picture taken after the C4 plasma exposure exhibits a complex pattern: poloidal striped lines on the left side, quite homogeneous aspect in the middle part of the MB and remaining damage marks on the right side of the MB. Toroidal cracks also appears near the 1 mm chamfer of the pre-damaged PFU and also near the sharp leading edge on the next PFU (#8) as already reported in [14,24].

The temperature profiles extracted from the IR image along the poloidal and toroidal directions are displayed in Fig. 9 for two similar pulses, one of the first (red) and one of the last (blue) pulse of the dedicated exposure sessions. On the poloidal profile (a), we observe temperature decays in both, private (left) and SOL (right) areas, suggesting a quite peaked heat load profile compared to the MB width (12 mm). The temperature found in the toroidal gaps (0.5 mm width) exhibits higher values due to the cavity effect (local increase of the emissivity in the gap because of the multi-reflexion on the two MB sides facing each other). Consequently, the absolute temperature values obtained in the gaps have no physical basis. However, such local increase of temperature is useful to localize the contour of the MB surface. The peak temperature is localized at $\times = 3$ mm from the toroidal gap for the two pulses, fully on the pre-damaged area (since only half of the MB was pre-damaged). The simulation gives S = 3 mm and λ_q = 8 mm on the target to reproduce the measurement as closely as possible (black line). The heat flux decay length derived from the VHR IR system being small compared to the one derived from standard diagnostics ($\lambda_q = 12 \pm 3$ mm is measured with standard IR thermography directly on the target, see Fig. 7-b), the peak heat load is consequently higher to keep the power received by the MB constant. About 5 MW.m^{-2} peak heat load is required to reach 370 °C on the top surface of the MB with 8 mm heat flux decay at the target (which is equivalent to 120 MW.m^{-2} parallel heat flux according to 1). The projection of the SOL heat flux decay length on the target is small compared to the MB width, consequently, the healthy part located on the low field side is colder (<350 °C) than the pre-damaged part of the MB located on the high field side and connected to the separatrix (~375 °C). No surface effect could be observed along the poloidal direction because of the small heat flux decay length (same heat flux would be required on both "pre-damaged" and "healthy" areas in order to make proper conclusion).

A temperature decrease of about 40 °C is observed between these two pulses, which is consistent with the reduction of power in the divertor of about 10 % and confirmed by the full set of embedded temperature sensors. Even if the injected power and plasma density are similar, the heat load on the divertor targets could be different because of the impurity content driving the radiated power, the residual MHD activity from the plasma start-up phase or the turbulence and heat transport properties, which could also be different from pulse to pulse. No surface evolution was therefore observed during the dedicated plasma exposure experiment.

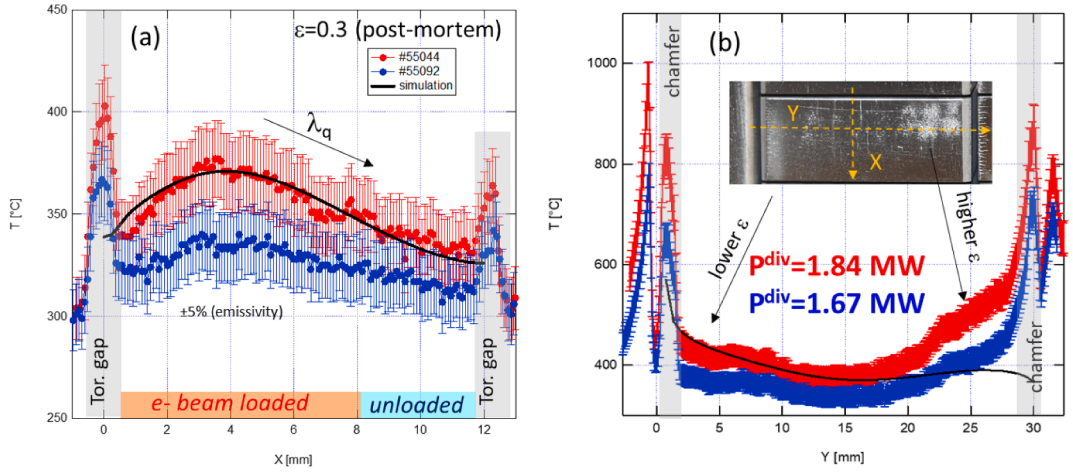

Fig. 9. Poloidal (a) and toroidal (b) temperature profiles obtained during the dedicated plasma exposure experiment at the beginning (in red) and the end (in blue) of the experimental sessions, assuming constant emissivity (0.3) over the MB surface. Surface temperature obtained with ANSYS simulation (v = 10 m/s, P = 3 MPa, T°=70 °C), assuming 10 % surface exposure on the chamfer, is shown in black.

On the toroidal profiles (b), curved temperature profiles are observed as expected from the heat transfer modelling because of the location of the cooling pipe in the middle of the MB. The experimental temperatures of the chamfers are 850 °C and 900 °C on the leading and trailing edges, respectively, assuming the same emissivity as measured on the top surface (0.3). Such evaluation is not accurate here because of the parasitic light emitted near the pre-damaged block and reflected on the 1 mm chamfer, due to its inclination (45°), toward the IR camera detector located on the top of the machine as depicted in [25]. The adjacent PFUs, uncooled W-coated graphite component on the previous (#6) and misaligned sharp leading edge component on the next PFU (#8) exhibit high surface temperature, which therefore provides significant reflection near the 1 mm chamfers. Contrary to the ANSYS simulation (black curve), the surface temperature derived from IR data is higher on the trailing (right hand side) versus leading edge (left hand side), which is consistent with the surface observation and emissivity measurements (see Fig. 1 and [21]) performed after the plasma exposure: the pre-damaged pattern is still visible and the surface emissivity is higher ($\varepsilon \sim 0.4$) on the right and smaller on the left (near the leading edge $\varepsilon < 0.1$).

Post-mortem measurement: Confocal microscopy

The test divertor sector that includes the pre-damage component was removed from the WEST device after the C4 experimental campaign. The actively cooled ITER like components have been removed from the test divertor sector and replaced by brand new components featuring the same shaping as foreseen in ITER (0.5 mm toroidal bevel) to prepare the transition to the fully actively cooled divertor WEST phase II. This provides the opportunity to perform post-mortem analysis on the pre-damaged areas. Results obtained with confocal microscopy on the full MB top surface are shown in Fig. 10 (x5 magnification). As also depicted in [6], the measurement performed directly after pre-damage (figure a) exhibits darkened areas in well-defined patterns corresponding to the impact of the electron beam on the surface. After plasma exposure (figure b), the pre-damage pattern is still visible with an improved contrast, probably because of the plasma polishing effect due to the erosion processes. Meanwhile, we observed broadening of the existing cracks and new cracks (as pointed in red, mostly on the right side of the MB, near the un-loaded area). The cracks are perpendicular to the MB top surface, therefore parallel to the elongated W-grains, which are within the Z direction as foreseen in ITER. Near the leading edge, we can see several new and broad cracks in both e-beam loaded and unloaded areas (as pointed in orange), which is consistent with previous post-mortem observation made on misaligned PFUs [26]. Consequently, the cracking observed on the poloidal leading edge cannot be directly related to the e-beam loading. As demonstrated numerically, it could be explained by over stress accumulated during disruptions, leading to brittle failure [24].

To check if the new cracks are related to the pre-damage, similar measurement performed with confocal microscopy has been carried out on the top surface of another PFU (healthy-one, PFU #9) located in similar heat loading area (Fig. 3). No cracking on the top surface of these MBs were detected, which indicates that the observation made on the pre-damage PFU (#7) is valid only for electron beam loaded areas.

To highlight the crack damage evolution after plasma exposure, Fig. 11 displays confocal measurements performed with higher magnification (x20) in two areas of interest in the MB surface. Zoom 1 is localized on the right side of the MB in the poloidal direction (on the outboard side of the tokamak) and centered on the frontier between e-beam loaded and unloaded areas (see Fig. 10-b). Zoom 2 is localized in the middle of the MB surface, looking on the e-beam loaded area only

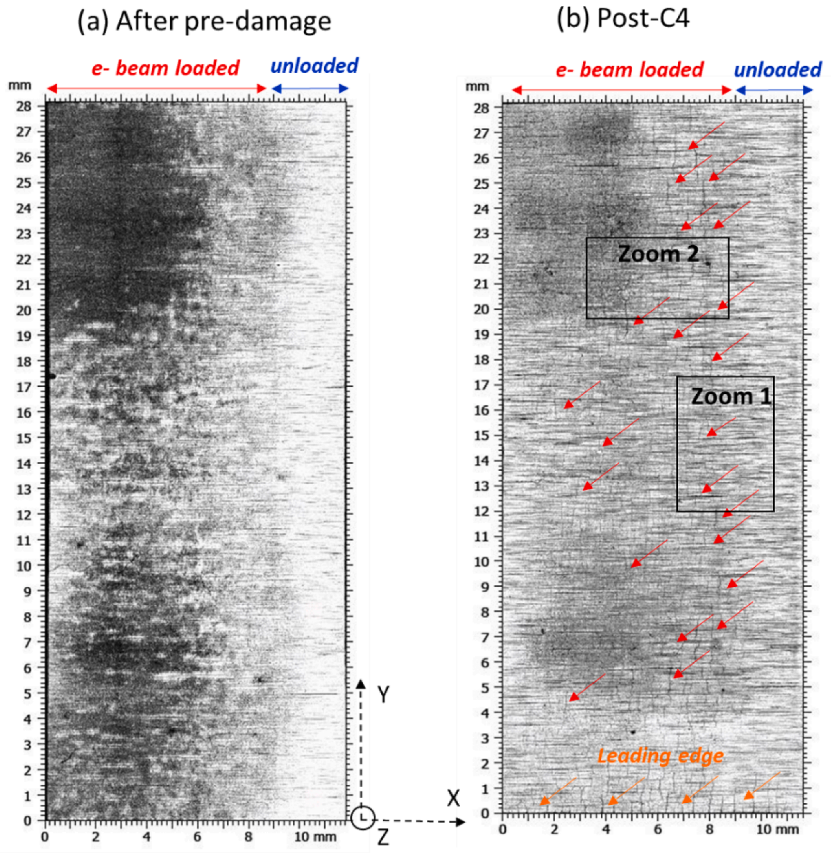

Fig. 10. Confocal microscopy performed before (a) 2017 and after (b) 2021 tokamak exposure (spatial sampling is 2.58 μm). The measurement area is shown on the right (X and Y are poloidal and toroidal direction, respectively).

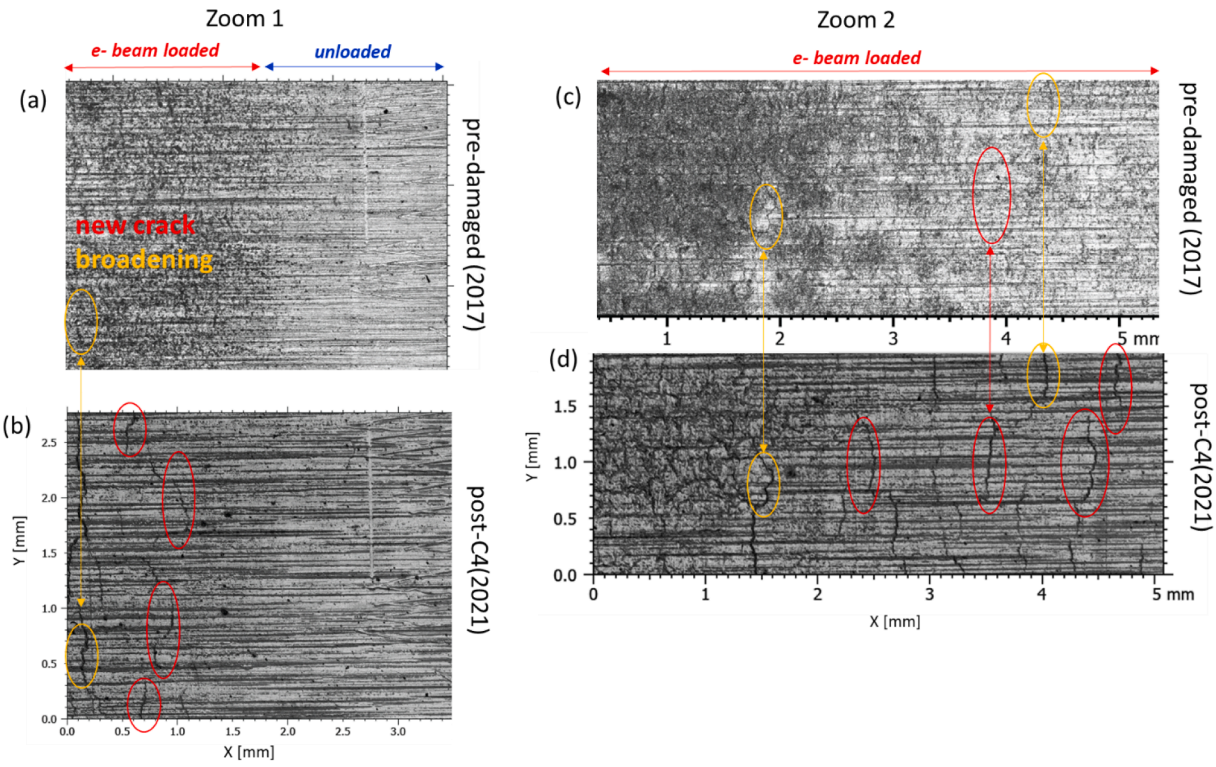

Fig. 11. Middle right side (Zoom 1) and upper center (Zoom 2) confocal imaging (x20 magnification, spatial sampling = 645 nm). Before on top (2017) and after on bottom (2021) tokamak exposure (X and Y are poloidal and toroidal direction, respectively).

(see Fig. 10-b). On the post-C4 measurements (bottom images Fig. 11), we clearly see crack broadening and propagation. The crack propagates mainly in the toroidal direction (Y axis) up to a millimeter length. The crack width is typically several micrometers (few micrometers on the top surface and few tens of micrometers on the leading edge where cracks are much broader). New cracks are also detected in the e-beam loaded areas only (see red contours). However, it is important to note that the cracks were more difficult to detect directly after the pre-damage process because of the machining grooves generated by the block manufacturing process and also because of the darkened effect corresponding to the impact of the electron beam on the surface as depicted in [6]. In zoom 1, right side, not loaded by the electron beam gun ("healthy" area), we don't observe any new crack. This further confirms the previous statement based on the confocal measurement performed on PFU #9 ("healthy"). Thermomechanical modelling and further post-mortem analysis are required to describe and characterize the crack evolution in a more proper way.

Conclusion

A robust steady state plasma scenario has been developed ($P^{inj} = 4$ MW, $I_p = 500$ kA, $B = 3.7$ T) in WEST to maximize the power and energy load on the pre-damaged MBs featuring the crack network pattern. About 600 s exposure time with significant steady state heat load on the damaged area top surface have been reached using the same magnetic equilibrium and plasma setting. No consequence on the plasma radiation, from the global point of view with the total radiated power and also from a local point of view with the WI emission sources, were observed during the successive plasma discharges, so that the pre-damaged area did not hinder the plasma operation. The heat load derived from standard and high spatial resolution (VHR IR system) diagnostics exhibit large discrepancy, 2.5 MW.m^{-2} or 5 MW.m^{-2} assuming broad or narrow heat flux decay lengths, respectively. On the micrometer scale in the crack cavity, the parallel heat flux impinging the crack could be more intense (~60 or 120 MW.m^{-2} assuming broad or narrow heat flux decay lengths, respectively) because of the quasi-normal incident angle of the magnetic field lines with the exposed poloidally-running leading edges (cracks featuring poloidal extension). Using the emissivity post-mortem measurement (0.3 mean value, with standard deviation ± 0.02) and VHR IR data collected during the experiment, we estimate the temperature on top surface of the damaged area to be 350 °C (at the center of the MB) and higher near the 1 mm chamfer. Reduction of the power dissipated through the divertor (10 %) and heat load reported on the divertor target (10 % as well) are observed during the dedicated plasma exposure using the same injected power and plasma equilibrium. This is consistent with 40° temperature reduction also observed with the VHR IR system. No surface evolution has been observed or noticed during the dedicated plasma exposure. Confocal measurements performed before installation and after removal of the PFU shows broadening and propagation of the cracks, mainly in the toroidal direction. New cracks are also detected after the full plasma exposure including steady state and significant number of transient heat loads due to disruptions as reported during the C3 and C4 experimental campaigns. Further post-mortem and thermomechanical analysis are planned to confirm this results and try to explain the mechanism involve in such evolution of the pre-damage.

CRediT authorship contribution statement

Yann Corre: Formal analysis. **Torsten Loewenhoff:** . **Marianne Richou:** Conceptualization. **Sebastijan Brezinsek:** Supervision. **Jan Coenen:** Supervision. **Renaud Dejarnac:** Formal analysis. **Mathilde Diez:** Formal analysis. **Nicolas Fedorczak:** Formal analysis. **Mehdi Firdaouss:** Formal analysis. **Jonathan Gaspar:** Formal analysis. **Alex Grosjean:** Investigation. **James-Paul Gunn:** . **Thierry Loarer:** . **Céline Martin:** Investigation. **Gerald Pintsuk:** . **Pierre Reilhac:** Investigation. **Quentin Tichit:** Investigation. **Emmanuelle Tsitrone:** Supervision. **Marius Wirtz:** . **the WEST team:** .

Declaration of Competing Interest

The authors declare that they have no known competing financial interests or personal relationships that could have appeared to influence the work reported in this paper.

Data availability

Data will be made available on request.

Acknowledgment

"This work has been carried out within the framework of the EUROfusion Consortium, funded by the European Union via the Euratom Research and Training Programme (Grant Agreement No 101052200 — EUROfusion). Views and opinions expressed are however those of the author(s) only and do not necessarily reflect those of the European Union or the European Commission. Neither the European Union nor the European Commission can be held responsible for them."

References

[1] R.A. Pitts, et al., Physics basis for the first ITER tungsten divertor, Nucl. Mater. Energy 20, no. February (2019), 100696, https://doi.org/10.1016/j.nme.2019.100696.
[2] ITER, "ITER Research Plan within the Staged Approach (Level III – Provisional Version)" 2018.
[3] J. Bucalossi et al., "The WEST project: Testing ITER divertor high heat flux component technology in a steady state tokamak environment," Fusion Eng. Des., vol. 89, no. 7–8, 2014, 10.1016/j.fusengdes.2014.01.062.
[4] C. Linsmeier, et al., Material testing facilities and programs for plasma-facing component testing, Nucl. Fusion 57 (9) (Jun. 2017), https://doi.org/10.1088/1741-4326/aa4feb.
[5] P. Majerus, R. Duwe, T. Hirai, W. Kühnlein, J. Linke, and M. Rödig, "The new electron beam test facility JUDITH II for high heat flux experiments on plasma facing components," Fusion Eng. Des., vol. 75–79, no. SUPPL., pp. 365–369, 2005, 10.1016/j.fusengdes.2005.06.058.
[6] M. Richou et al. « First plasma exposure of a pre-damaged ITER-like plasma-facing unit in the WEST tokamak: procedure for the PFU preparation and lessons learned" 2022 Nucl. Fusion 62 056010. https://iopscience.iop.org/article/10.1088/1741-4326/ac412e.
[7] M. Balden, et al., Erosion and redeposition patterns on entire erosion marker tiles after exposure in the first operation phase of WEST, Phys. Scr. 96 (2021), 124020, https://doi.org/10.1088/1402-4896/ac2182.
[8] J. Gaspar, et al., Emissivity measurement of tungsten plasma facing components of the WEST tokamak, Fusion Eng. Des. 149 (2019), 111328, https://doi.org/10.1016/j.fusengdes.2019.111328.
[9] M. Missirlian, et al., The WEST project: Current status of the ITER-like tungsten divertor, Fusion Eng. Des. 89 (7) (Oct. 2014) 1048–1053, https://doi.org/10.1016/j.fusengdes.2014.01.050.
[10] Y. Corre, et al., Sustained W-melting experiments on actively cooled ITER-like plasma facing unit in WEST, Phys. Scr. 96 (2021), 124057.
[11] J. Bucalossi et al. "Operating a full tungsten actively cooled tokamak: overview of WEST first phase of operation". 2022 Nucl. Fusion 62 042007.
[12] P, Moreau,, et al., Measurements and controls implementation for WEST, Fusion Eng. Des. 123 (November 2017) 1029–1103, https://doi.org/10.1016/j.fusengdes.2017.01.046.
[13] J. Gaspar et al. "Divertor power loads and scrape off layer width in the large aspect ratio full tungsten tokamak WEST". Nucl. Fusion 61 096027. 10.1088/1741-4326/ac1803.
[14] J. Gunn, et al., Thermal loads in gaps between ITER divertor monoblocks: First lessons learnt from WEST, Nuclear Materials and Energy 27 (June 2021), 100920.
[15] M. Firdaouss, et al., Heat flux depositions on the WEST divertor and first wall components, Fusion Eng. Des. 98–99 (2015), https://doi.org/10.1016/j.fusengdes.2014.12.024.
[16] E. Tsitrone et al. "Investigation of plasma wall interactions between tungsten plasma facing components and helium plasmas in the WEST tokamak", Nuclear Fusion 10.1088/1741-4326/ac2ef3.
[17] O. Meyer, et al., « Visible spectroscopy diagnostics for tungsten source assessment in the WEST tokamak: First measurements", Rev. Sci. Instrum. 89 (2018) 10D105, https://doi.org/10.1063/1.5035566.
[18] J. Gaspar, et al., Surface heat flux estimation with embedded fiber Bragg gratings measurements: Numerical study, Nucl. Mater. Energy 12 (2017) 1077–1081, https://doi.org/10.1016/j.nme.2016.10.015.
[19] N. Fedorczak, et al., Cross diagnostics measurements of heat load profiles on the lower tungsten divertor of WEST in L-mode experiments, Nuclear Materials and Energy. 27 (June 2021), 100961, https://doi.org/10.1016/j.nme.2021.100961.
[20] T. Hirai, et al., Design optimization of the ITER tungsten divertor vertical targets, Fusion Eng. Des. 127 (February 2018) 66–72, https://doi.org/10.1016/j.fusengdes.2017.12.007.
[21] M. Houry, et al., The very high spatial resolution infrared thermography on ITER-like tungsten monoblocks in WEST Tokamak, Fusion Eng. Des. 146 (Sep. 2019) 1104–1107, https://doi.org/10.1016/j.fusengdes.2019.02.017.
[22] J. Gaspar et al. Overview of the emissivity measurements performed in WEST: in-situ and post-mortem observations. Nuclear Fusion, accepted.
[23] Y. Corre et al. "Methodology for heat flux investigation on leading edges using infrared thermography". Nucl. Fusion 57 (2017) 016009 (9pp).
[24] A. Durif et al. "Leading edge cracking observed in WEST" 2022 Phys. Scr. 97 074004.
[25] A. Grosjean, et al., Interpretation of temperature distribution observed on W-ITER-like PFUs in WEST monitored with a very-high-resolution IR system, Fusion Eng. Des. 168 (2021), 112387.
[26] M. Diez et al. "In situ observation of tungsten plasma-facing components after the first phase of operation of the WEST tokamak" 2021 Nucl. Fusion 61 106011. 10.1088/1741-4326/ac1dc6.